**Title**

A semi-automated phenotypic *in vitro* scratch assay for assessing retinal pigment epithelial cell wound healing

**Authors:**

Tina Storm(1) *, Iain Wilson (1), Ross Campbell (1), Arantxa Bolinches-Amorós(1), Angela J. Russell(3,4), Stephen G. Davies(3), Alun R Barnard(1,2) and Robert E. MacLaren(1,2) *

**Affiliation:**

(1)Nuffield Laboratory of Ophthalmology, Department of Clinical Neurosciences, John Radcliffe Hospital, Level 5 & 6, West Wing, Headley Way, OX3 9DU, UK

(2)Oxford Eye Hospital, Oxford University Hospitals NHS Trust, John Radcliffe Hospital, West Wing, Headley Way, OX3 9DU, UK

(3)Department of Chemistry, Chemistry Research Laboratory, Mansfield Road, University of Oxford, Oxford, OX1 3TA, UK

(4)Department of Pharmacology, Mansfield Road, University of Oxford, Oxford, OX1 3PQ, UK

**Running title:** Retinal pigment epithelium wound healing assay

**Keywords:** Retinal pigment epithelium, Age-related macular degeneration, Geographic atrophy, wound healing assay

*** Correspondence to:**

Robert E. MacLaren

Nuffield Laboratory of Ophthalmology, Department of Clinical Neurosciences, John Radcliffe Hospital, Level 5 & 6, West Wing, Headley Way, OX3 9DU, UK

Email: enquiries@eye.ox.ac.uk

Tina Storm

Nuffield Laboratory of Ophthalmology, Department of Clinical Neurosciences, John Radcliffe Hospital, Level 5 & 6, West Wing, Headley Way, OX3 9DU, UK

Email: tinastorm83@gmail.com

**Abstract**

**Purpose**

Age-related macular degeneration leads to retinal pigment epithelium (RPE) cell death and loss of central vision. *In vivo* studies have shown that the RPE layer has an innate but limited ability to repopulate atrophic areas. We aimed to establish a semi-automated *in vitro* wound healing assay workflow for targeted screening of compounds able to influence RPE wound healing.

**Methods**

ARPE-19 phenotype was evaluated using bright field microscopy, immunocytochemistry, and qRT-PCR. ARPE-19 monolayers were simultaneously scratched in a 96-well format, treated with Hoechst-33342 and an array of compounds. Initial wound dimensions and wound healing were subsequently evaluated using EVOS FL auto 2.0 imaging platform combined with automated image analyses.

**Results**

Long-term cultured ARPE-19 cells displayed a more *in vivo* RPE-like phenotype compared to recently seeded or short-term cultured cells. No statistical difference of initial scratch width was observed between short-term and long-term cultured cells but more wells were excluded from analyses in total in the latter case due to scratch width, scratch smoothness and imaging errors. Furthermore, the previous time spent in continuous culture had an effect on the observation of an altered wound healing response to different treatment conditions.

**Conclusions**

We have established a semi-automated, 96-well format, *in vitro* wound healing assay with a reproducible workflow. This would enable screening of a significant number of compounds, and greatly advances the potential of identifying novel therapeutics that may enhance the innate ability of the RPE cells to repopulate atrophic areas.

## Introduction

Age-related macular degeneration (AMD) is the leading cause of blindness in the elderly population of developed countries[1]. It is a complex disorder with contribution from both genetic and environmental factors. The early stages of AMD are characterised by the appearance of small subretinal deposits called drusen[2]. As the size and confluence of these increase, the disease progresses to a more severe and advanced stage. There is progression into either a vascular ('wet') form, where newly formed vessels grow through the retinal pigment epithelium (RPE) layer into the subretinal space causing rapid loss of central vision, or into an avascular ('dry') form, known as geographic atrophy, where the RPE cells of the macular region are lost. Several pathological pathways are believed to be associated with geographic atrophy, including aberrant regulation of the complement system, accumulation of lipofuscin, oxidative damage, and chronic inflammation[2]. These have adverse effects on RPE function leading to the loss of macular RPE cells and ultimately loss of central vision due to a secondary loss of the overlying photoreceptors.

Current therapeutic approaches to treating dry AMD are focused on preventing or slowing down disease progression targeting known cellular pathologies at the earlier stages of the disease and an increasing number are reaching clinical trial stages[3]. In contrast, efforts to repopulate macular atrophic areas of RPE have focused on cellular regenerative therapies with transplantation of healthy RPE cells derived from a number of stem cell sources into the atrophic macular region. A number of clinical trials are ongoing, however so far only with limited success[4].

Central RPE cells of the mammalian retina are non-proliferative under normal conditions but are able to proliferate under certain pathological conditions, such as proliferative vitreoretinopathy but also after laser photocoagulation, a widely used treatment for various retinal disorders. Furthermore, endogenous RPE regeneration has been recently reported; in zebrafish after genetic ablation of adult RPE cells[5] and in mice after chemical injury[6,7]. Overall, this suggests that the intrinsic regenerative potential found in some lower vertebrates may be latent but still present in the adult mammalian eye.

Interestingly, gene transfer of the *E2F2* transcription factor induced increased RPE proliferation and central RPE density in a transgenic mouse model of RPE cell loss[8] suggesting that *in situ* RPE restoration could be possible. Ideally, controlled RPE regeneration will one day be achievable through small molecule induction of the latent proliferative potential of the macular RPE cells, thereby averting or even reversing disease progression. As the life expectancy of the population increases, so does the prevalence of AMD, and the number of patients is predicted to surpass 280 million people globally within the next 20 years[1]. Thus, there is an important and growing need for good phenotypic *in vitro* models and assays to develop novel therapeutic approaches.

The scratch/wound healing assay is particular well suited as an *in vitro* model for repopulation of the atrophic macular region. Numerous wound healing assays have been reported in the literature and readers are directed towards detailed reviews that discuss the different techniques for wound creation (mechanical, electrical, chemical or thermal), wound healing monitoring (transmitted light, fluorescence) and their relative merits as *in vitro* models for compound testing[9-11]. Unfortunately, none of the previously reported methods are good for reproducible screening with a significant throughput using biologically relevant RPE cells. To our knowledge there are no previous reports of 96-well format wound healing assay suitable for RPE wound healing investigations.

Here, we describe a biological relevant *in vitro* wound healing assay appropriate for screening of a significant number of compounds for biological activity. We demonstrate reproducible scratch introduction in a 96-well format, as well as automated image acquisition and analyses. This enables phenotypic evaluation of molecules in a semi-automated manner, thus increasing the potential to identify novel therapeutics that may enhance the innate ability of the RPE cells to repopulate atrophic areas.

## Methods

### Cell Culture

ARPE-19 cells were purchased from American Type Culture Collections (CRL-2302, ATCC, Manassas, VA). Cells were seeded at a density of 90,000 cells/cm$^2$ and maintained in a humidified incubator at 37°C with 5% $CO_2$ and initially seeded in Dulbecco's Modified Eagle's Medium (DMEM)/F12 (31331093, Thermo Fisher Scientific, Paisley, UK) supplemented with 10% heat-inactivated foetal bovine serum (10500-064, Thermo Fisher Scientific), and 1% penicillin/streptomycin (P4333-100ML, Sigma-Aldrich (Merck), Dorset, UK). Cells were subsequently maintained in DMEM with high glucose (4.5 g/L) and pyruvate (41966052, Thermo Fisher Scientific) supplemented with 1% heat-inactivated foetal bovine serum and 1% penicillin/streptomycin. Culture medium was exchanged twice weekly.

### Quantitative real time polymerase chain reaction (qRT-PCR).

Cells were seeded in Corning™ Primaria™ 6-well plates (353846, Scientific Laboratory Supplies, Nottingham, UK). Total RNA was extracted from cells using the miRNeasy Mini Kit (217004, Qiagen, Manchester, UK) following manufacturer recommendations. 1 μg of total RNA was reverse transcribed using the QuantiTect Reverse Transcription kit (Qiagen). 20 ng of cDNA were used as a template for each qRT-PCR reaction using specific TaqMan® (Thermo Fisher Scientific) probes (Table 1). The thermal cycling conditions were 10 min at 95°C followed by 40 cycles of 15 s at 95°C and 1 min at 60°C. *GAPDH* was used as the reference gene. The results were expressed as n-fold change in gene expression relative to the non-differentiated cells calculated using the ΔΔCt method. A Two-way ANOVA was used to test for statistically significance, with differentiation time and gene identity as the two factors.

### Immunocytochemistry

Cells were seeded in Corning™ Primaria™ 96-well plates (353872, Scientific Laboratory Supplies) and maintained as described above. Cells were washed twice with pre-warmed phosphate-buffered

saline (PBS), and fixed in 4% methanol-free formaldehyde (28906, Thermo Fisher Scientific) for 15 minutes. Cells were subsequently permeabilised with 0.1 % Triton x-100 diluted in PBS supplemented with 1% bovine serum albumin (BSA) for 10 minutes at room temperature (RT) and incubated with rabbit anti ZO-1 (1:200) (617300, Thermo Fisher Scientific) at RT for 1 hour and visualised with secondary Goat anti Rabbit Alexa Fluor 488 (1:1,000) (A11008, Thermo Fisher Scientific). F-actin staining was performed with phalloidin-488 or phalloidin-555 (1:20) (A12379/A34055, Thermo Fisher Scientific) for 30 minutes and cell nuclei counter stained using Hoechst 33342. Bright field images were acquired using an inverted epifluorescence microscope (DMIL, Leica). Cellular immunofluorescence stainings were evaluated using the EVOS FL auto 2.0 imaging platform (Thermo Fisher Scientific) and images subsequently processed with Image J.

Scratch assay

Cells were seeded in Corning™ Primaria™ 96-well plates (353872, Scientific Laboratory Supplies) and maintained (as described above) for either three weeks or 4 months (2 plates per time point). Scratches were introduced simultaneously, centrally in the ARPE-19 monolayer in all 96 wells using the WoundMaker™ (Essen BioScience Ltd., Welwyn Garden City, UK) according to manufacturer's protocol. Cells were subsequently treated with either 5 ng/ml transforming growth factor- beta 1 (TGF-β1) (ab50036, Abcam, Cambridge, UK) or 10 uM (5*Z*)-7-oxozeaenol (5679, Tocris, Bristol, UK). These treatments were provided in DMEM supplemented with 1% KnockOut™ Serum Replacement (A3181501, Thermo Fisher Scientific),1% penicillin/streptomycin and Hoechst 33342 (1:20,000). *The non-treated control (NTC) group received culture media lacking treatment supplement and a dimethylsulfoxide (DMSO) treatment group received culture media with DMSO added to a final concentration of 0.1%***.** To avoid potential edge/plate positional effects, a different treatment plate map was used for each of the two plates. One hour post compound treatment, 96-well plates were transferred from the incubator to the EVOS FL auto 2.0 imaging platform for imaging of the central 50 % of the well areas in all 96 wells in an automatic fashion using the x4 objective and the DAPI channel to autofocus on the Hoechst 33342 stained nuclei. Four images were

acquired per well and tiled together (with no overlay) to one single image for evaluation of the initial scratch dimensions. Subsequently, the central 10 % of the well areas in all 96 wells were automatically imaged using the x10 objective and the DAPI channel to autofocus on the Hoechst 33342 stained nuclei. Four images were acquired per well and tiled together (with no overlay) to one single image for subsequent image processing and analysis. The central 10 % of the well areas in all 96 wells were subsequently imaged again at day 1, 2 and 3 for evaluation of wound healing rates.

Image processing

Custom image processing software was developed using python programming language, running on Apple OSX 10.14.2.

Original tiled images were pre-processed to produce a clean binary image. This was performed by using an adaptive thresholding technique, then a morphological opening operation was applied to remove noise. This binary image was then used as the input for the mask creation process; A substantial blur was applied, threshold and the morphological opening operation applied to remove noise. This produced a clean mask outlining the scratch area (Supplementary Figure 1).

Binary Image Creating Workflow:

a. Adaptive Thresholding
b. Morphological Opening

Mask Creation Workflow:

a. Blur – 6 iterations, 21x21 size kernel
b. Thresholding
c. Morphological Opening

The resulting mask was used to segment the area of the original image for analysis. Cell density was estimated by counting the non-zero pixels within the masked scratch area. Heatmaps of cell density were generated to visualise the results. This was performed by first applying a box filter, histogram normalisation, and finally using a colour lookup table.

With the produced map, a measure of wound quality was generated. This was calculated with the three following parameters and wells were excluded based on this calculation.

1. The average width of the scratch. Small widths were rejected (<568 μm).
2. Density of cells within the mask area. High number of cells indicated poor scratch introduction.
3. Smoothness of scratch. Non-straight edges were associated with poor scratch introduction

The above process was repeated for each well, on the 96-well plates. Variability of the automated scratch process was calculated using the centre point and height from the scratch mask. Repeated measures were performed and expressed using the Bland-Altman coefficient of repeatability (CoR).

Equation 1. $CoR = sd * 1.96$

Where "sd" is the standard deviation of the measurement.

Wound healing was quantified using a measure of cell ingress into the scratched area. Using the scratch masks created on Day 0, the scratch area within the well was isolated and the local cell density for each time point was calculated.

## Results

*ARPE-19 phenotype assessment*

Bright field microscopy showed loosely packed, plump spindle-shaped cells in newly confluent ARPE-19 cells (Figure 1A) with non-defined cells borders and visible nuclei. This morphology slowly transformed with continuous culture without passage, through a more irregular cell shape with emerging defined cell borders, loss of visible nuclei (Figure 1B), into a densely packed, well defined layer of cells with cobblestone epithelial morphology (Figure 1C). In accordance with a more differentiated RPE phenotype, substantial pigmentation was also observed in cell patches in most wells (Figure 1C). Immunocytochemical visualisation of the tight junction protein zonula occludens-1 (ZO-1) showed a more uniform cell membrane distribution in short-term cultured and long-term cultured ARPE-19 cells when compared to the newly confluent cells (Figure 1D, E and F). Furthermore, the distribution of filamentous actin (F-actin) was predominantly observed in circumferential bundles in the long-term cultured ARPE-19 cells compared to the newly confluent and short-term cultured ARPE-19 cells where the actin filaments were observed in a stress type-fibre pattern as well as circumferential bundles in the majority of cells (Figure 1G, H and I).

Quantitative gene expression analyses of selected markers associated with a RPE phenotype (Figure 2) showed that prolonged culturing of the ARPE-19 cells resulted in an increasingly biological relevant RPE phenotype over time. Statistically significant increase in expression levels of genes associated with the visual cycle (*RPE65*, *RLBP1*), RPE cell function (*BEST1*, *MERTK*), pigmentation (*TYR, TRPM3*), RPE differentiation (*MITF*), and tight junctions (*TJP1*) was associated with prolonged culture and differentiation of the ARPE-19 cells when compared to the newly seeded cells. Combined, this confirms that prolonged culturing of ARPE-19 cells produces a more *in vivo* RPE-like phenotype and that these cells are therefore a more biologically relevant *in vitro* model than newly seeded ARPE-19 cells.

*Evaluation of scratch consistency*

In order to evaluate the consistency of the wound dimensions introduced in ARPE-19 cell monolayers we measured the median scratch width using a custom-made image processing workflow and tested for statistical significance (Kruskal-Wallis test) in scratch width between plates (Figure 3 and supplementary figure 2A). The median scratch width was 802 pixels with an inter quartile range of 59 pixels. No statistical difference of scratch width was observed between plates. Furthermore, visual inspection of the images obtained using the automated imaging platform showed reliable image quality and the algorithm for automated scratch segmentation showed consistency with manual visual inspection of analysed images (supplementary figure 2A).

Based on the scratch segmentation, 113/192 wells (59%) were excluded from analysis in the long-term cultured cells compared to 86/192 wells (45%) in the short-term cultured cells (Figure 3) based on scratch width, scratch smoothness and imaging errors. More wells were excluded based on wound width and/or wound smoothness in the long-term cultured cells than in the short-term cultured cells (Figure 3) suggesting that scratch introduction is less consistent in more established and differentiated monolayers of ARPE-19 cells.

*Investigation of the wound healing process*

We investigated the wound healing process in a number of treatment conditions to evaluate the robustness of the total workflow from scratch introduction to image processing as well as the overall biological relevance of the *in vitro* system. The dependent variable, 'wound healing' was tested for normality, for each condition. Using the Shapiro-Wilk test for normality, it was found to be significantly different from a normal distribution. Thus, the Kruskal-Wallis test was used to compare 'wound healing' for the different conditions. The Kruskal-Wallis rank sum test provided strong evidence of a difference ($p < 0.0001$) in mean wound healing at day 2 for a number of the conditions tested. Dunn's pairwise tests were carried out for the four conditions and showed (adjusted using the Bonferroni correction) a significant difference between the following pairs in the short-term

differentiated cells; NTC v DMSO-0.1% ($p<0.0001$) and NTC v TGF-β1 ($p<0.0001$) (Figure 4B) whereas the following pairs showed a significant difference in the long-term cultured cells; NTC v (5*Z*)-7-oxozeaenol ($p=0.001$) and DMSO-0.1% v (5*Z*)-7-oxozeaenol v ($p<0.0001$) (Figure 5B).

Inspection of heat maps visualising nuclear density in the region of interest (10% central well area) generally showed a higher nuclei density at day 0 compared to subsequent days for both short-term and long-term cultured cells (Figure 4A and 5A) suggesting that cellular migration into the wounded area is a major contribution to wound healing. Furthermore, the nuclei density of short-term differentiated ARPE-19 cells appears to be visibly lower than the nuclei density of prolonged differentiated ARPE-19 cells (supplementary figure 3). Correlation of the heat map high density areas in the prolonged ARPE-19 wells to the corresponding areas on bright field images furthermore showed that they reflect patches of highly differentiated ARPE-19 cells displaying both cobblestone morphology and advanced pigmentation (supplementary figure 3).

**Discussion**

The wound healing assay is an established and recognised *in vitro* assay and has been widely used to investigate basic cellular mechanisms as well as assessment of pharmacological intervention in a vast number of cell types. However, the assay is not without shortcomings, due to issues with standardisation, accuracy and reproducibility[9,10]. In an RPE context, the assay has in particular been applied to investigate basic RPE mechanisms, pathological molecular mechanisms underlying proliferative vitreoretinopathy, as well as evaluating effects of potential therapeutic agents on the migratory and proliferative abilities of the RPE cell[12-21]. Here, we describe a biologically relevant 96-well format, *in vitro* wound healing assay with a reproducible workflow. Using the techniques, conditions and workflow described here we were able to simultaneously introduce RPE monolayer wounds in a 96-well format, perform automated image acquisition and automated image analysis whilst using an immortalised human RPE cell line with a biological relevant phenotype. When applied together, d this represents a significant advancement of the RPE *in vitro* wound healing assay compared to previous work which has predominantly been performed in a 6-well format (or comparable tissue culture surface area) using pipette tips for manual scratch introduction as well as manual image acquisition and analysis. Manual scratch introduction is not only substantially more time consuming and laborious, but would also most certainly lead to a significantly higher variability in intra-well scratch localisation as well as scratch dimensions, leading to a higher rate of well rejection to achieve a similar level of consistency as applied here.

The Radius™ 96-Well Cell Migration Assay (Cell Biolabs Inc.), a commercially available alternative to using the 96-well WoundMaker™ (Essen BioScience) for scratch introduction into established monolayers of cells. Unfortunately, the hydrogel used to exclude cells from populating a central area in the wells is not stable long-term when exposed to culture media and thus not compatible with epithelialisation/differentiation of ARPE-19 cells. In addition, using the Radius Migration Assay™ would furthermore constitute a significant continuous expense compared to the one-time expense of

acquiring the Essenbio Woundmaker. To our knowledge there are no alternative wound healing assays in a ≥96-well format that are suitable for the study of RPE wound healing.

Previous work on RPE *in vitro* wound healing has used primary RPE cells from a number of sources (including human[13,18], bovine[12] and porcine[17]) as well as induced pluripotent stem cell-derived RPE cells[19] and immortalised human RPE cell lines, such as ARPE-19[14,15,20,22,23] and D407[16]. The use of primary RPE cells for any *in vitro* assay that hopes to test a library of compounds or other supplements is far from ideal: substantial cell batch variation and ethical, time and cost considerations would likely limit the throughput and scale significantly. However, using immortalised human RPE cells such as ARPE-19[24] cells may lead to a significant compromise on the RPE phenotype[25-27], and thus biological relevance. Previous studies investigating RPE wound healing *in vitro* have predominantly used the cells in a newly confluent state where the RPE cells are still displaying a mesenchymal-like phenotype[28]. This RPE phenotype is indeed highly relevant for evaluating therapeutics that may prevent or halt proliferative vitreoretinopathy but it is suboptimal for mimicking the phenotype of cells within the *in vivo* epithelial monolayer.

By long-term culturing of the ARPE-19 cells (according to recently published guidelines[26,27]) we observed a gradual epithelialization, pigmentation and increased expression of proteins specific for RPE function, suggesting a biologically relevant phenotype of the ARPE-19 cells used in our wound healing assay. Interestingly, a larger number of wells were excluded based on wound width and/or wound edge smoothness in the long-term cultured cells compared to the short-term differentiated cells. This difference is most likely due to more established epithelial cell-cell junctions and integral association with the underlying extracellular matrix in the more differentiated cells, as the cells appeared to be displaced in larger coherent patches resulting in ragged wound edges. Smooth wound edges are paramount for achieving reproducible wound healing[10], suggesting that the use of long-term cultured cells is not optimal for consistent and reproducible scratch introduction. Despite the need to exclude a rather high number of sub-optimal wounds, using the Essen Bioscience woundmaker is still a very significant improvement to the user biased manual scratch introduction reported in previous

RPE wound healing assays. Most importantly it enables simultaneous scratch introduction in a 96-well format and prepares a significant number of wounded 96-well plates within a very short time, rendering the necessity of sub-optimal wound exclusion less significant overall.

Although the prolonged culturing of the ARPE-19 cells resulted in a further differentiated and more relevant RPE phenotype, we observed a clear intra-well and inter-well variation in individual RPE cell phenotype, based on differences in pigmentation and cobblestone cell morphology. Achieving a reproducible and consistent cell phenotype within wells, between wells and between plates, is of crucial importance for a reliable wound healing assay with low variance. This suggests that prolonged culturing of ARPE-19 cells is not optimal if the goal is to achieve a high throughput screening with an *in vitro* wound healing assay. In contrast, we observed less variation in wound width and scratch smoothness in the short-term cultured cells suggesting that these cells may be more appropriate for a high throughput setting.

Interestingly, the response of the short-term and long-term cultured cells appeared to be somewhat different when treated with the epithelial-to-mesenchymal inducer TGF-β1or the epithelial-to-mesenchymal inhibitor (5*Z*)-7-oxozeaenol. The short-term cultured cells displayed a significantly enhanced wound healing in the presence of TGF-β1 whereas the long-term cultured cells only displayed a tendency that did not reach statistical significance. In contrast, only the long-term cultured cells showed a significant inhibition of wound healing when treated with (5*Z*)-7-oxozeaenol. This may be a reflection of the observed differences in RPE phenotype of the cells. In short, the long-term cultured cells appear to have a more epithelial phenotype and may consequently be less sensitive to TGF-β1 resulting in a non-significant difference in wound healing rates and likewise for the short-term cultured cells being less epithelial and consequently less sensitive towards epithelial-to-mesenchymal inhibition.

Surprisingly, treatment of the short-term cultured cells with 0.1% DMSO, the standard solvent used for drug screening, showed a significant increase in wound healing compared to non-treated cells. This suggests that DMSO may be able to induce epithelial-to-mesenchymal in short-term cultured ARPE-19 cells and furthermore that caution and strict use of appropriate controls is needed if DMSO is used as vehicle in drug screening in this context. Thus, vigilance must be applied in choosing the RPE phenotype as well as the screening vehicle most appropriate for the specific screening goal in order to obtain the optimal wound healing assay.

The mammalian RPE layer has an innate but limited ability to repopulate atrophic areas[28]. *In vivo* studies have shown that the RPE regeneration occurs from the wound periphery towards the centre of the lesion[5,29]. More specifically, a detailed scanning electron microscopy and transmission electron microscopy study of RPE wound healing in a rabbit model[29] suggests that the cells at the margin of the lesion transition into an enlarged, flattened migratory phenotype and that the cells reverted back to an epithelial phenotype after wound closure. This supports that the ARPE-19 cells behave in an *in vivo* relevant manner in our wound healing assay as we observed related changes in morphology in the cells at the wound edges as they invade the acellular area.

In conclusion, we have established a biologically relevant and reproducible *in vitro* wound healing assay, appropriate for targeted screening of compounds with effects on RPE cell proliferation and migration. This enables quantitative phenotypic evaluation of molecules in an automated 96-well format greatly advancing the potential of identifying novel therapeutics that may enhance the innate ability of the RPE cells to repopulate atrophic areas.

**Acknowledgements**

This work was supported by a grant from OxStem Ltd.

The authors thank Federica Staurenghi, Nuffield Laboratory of Ophthalmology, University of Oxford for technical assistance.

**Author disclosure statement**

Tina Storm: No competing financial interests

Iain Wilson: No competing financial interests

Ross Campbell: No competing financial interests

Arantxa Bolinches-Amorós: No competing financial interests

Angela J. Russell: Founder and minor shareholder of OxStem Ltd.

Stephen G. Davies: Founder and minor shareholder of OxStem Ltd

Alun Barnard: No competing financial interests

Robert E. MacLaren: Grant funding from Oxstem Ltd

**Requests for reprints should be directed to**

Alun R Barnard

Nuffield Laboratory of Ophthalmology, Department of Clinical Neurosciences, John Radcliffe Hospital, Level 5 & 6, West Wing, Headley Way, OX3 9DU, UK

Email: alun.barnard@eye.ox.ac.uk

Telephone: +44 1865234701

References


1. Wong WL, Su X, Li X, et al. Global prevalence of age-related macular degeneration and disease burden projection for 2020 and 2040: a systematic review and meta-analysis. *The Lancet Global Health.* 2014;2(2):e106-e116.
2. Holz FG, Strauss EC, Schmitz-Valckenberg S, van Lookeren Campagne M. Geographic atrophy: clinical features and potential therapeutic approaches. *Ophthalmology.* 2014;121(5):1079-1091.
3. Taskintuna I, Elsayed ME, Schatz P. Update on Clinical Trials in Dry Age-related Macular Degeneration. *Middle East African journal of ophthalmology.* 2016;23(1):13-26.
4. Zarbin M, Sugino I, Townes-Anderson E. Concise Review: Update on Retinal Pigment Epithelium Transplantation for Age-Related Macular Degeneration. *Stem Cells Transl Med.* 2019.
5. Hanovice NJ, Leach LL, Slater K, et al. Regeneration of the zebrafish retinal pigment epithelium after widespread genetic ablation. *PLOS Genetics.* 2019;15(1):e1007939.
6. Xia H, Krebs MP, Kaushal S, Scott EW. Enhanced retinal pigment epithelium regeneration after injury in MRL/MpJ mice. *Exp Eye Res.* 2011;93(6):862-872.
7. Machalinska A, Kawa MP, Pius-Sadowska E, et al. Endogenous regeneration of damaged retinal pigment epithelium following low dose sodium iodate administration: an insight into the role of glial cells in retinal repair. *Exp Eye Res.* 2013;112:68-78.
8. Kampik D, Basche M, Luhmann UFO, et al. In situ regeneration of retinal pigment epithelium by gene transfer of E2F2: a potential strategy for treatment of macular degenerations. *Gene therapy.* 2017;24(12):810-818.
9. Ashby WJ, Zijlstra A. Established and novel methods of interrogating two-dimensional cell migration. *Integrative biology : quantitative biosciences from nano to macro.* 2012;4(11):1338-1350.
10. Jonkman JE, Cathcart JA, Xu F, et al. An introduction to the wound healing assay using live-cell microscopy. *Cell adhesion & migration.* 2014;8(5):440-451.
11. Sugino IK, Wang H, Zarbin MA. Age-related macular degeneration and retinal pigment epithelium wound healing. *Molecular neurobiology.* 2003;28(2):177-194.
12. Verstraeten TC, Buzney SM, Macdonald SG, Neufeld AH. Retinal pigment epithelium wound closure in vitro. Pharmacologic inhibition. *Investigative Ophthalmology & Visual Science.* 1990;31(3):481-488.
13. Kaida M, Cao F, Skumatz CM, Irving PE, Burke JM. Time at confluence for human RPE cells: effects on the adherens junction and in vitro wound closure. *Invest Ophthalmol Vis Sci.* 2000;41(10):3215-3224.
14. Lee H, O'Meara SJ, O'Brien C, Kane R. The role of gremlin, a BMP antagonist, and epithelial-to-mesenchymal transition in proliferative vitreoretinopathy. *Invest Ophthalmol Vis Sci.* 2007;48(9):4291-4299.
15. Takahashi E, Nagano O, Ishimoto T, et al. Tumor necrosis factor-alpha regulates transforming growth factor-beta-dependent epithelial-mesenchymal transition by promoting hyaluronan-CD44-moesin interaction. *J Biol Chem.* 2010;285(6):4060-4073.
16. Wang J, Yang Y, Xu J, Lin X, Wu K, Yu M. Pirfenidone inhibits migration, differentiation, and proliferation of human retinal pigment epithelial cells in vitro. *Mol Vis.* 2013;19:2626-2635.
17. Umazume K, Liu L, Scott PA, et al. Inhibition of PVR with a tyrosine kinase inhibitor, dasatinib, in the swine. *Invest Ophthalmol Vis Sci.* 2013;54(2):1150-1159.
18. Nagineni CN, Raju R, Nagineni KK, et al. Resveratrol Suppresses Expression of VEGF by Human Retinal Pigment Epithelial Cells: Potential Nutraceutical for Age-related Macular Degeneration. *Aging and disease.* 2014;5(2):88-100.
19. Por ED, Greene WA, Burke TA, Wang HC. Trichostatin A Inhibits Retinal Pigmented Epithelium Activation in an In Vitro Model of Proliferative Vitreoretinopathy. *Journal of*

*ocular pharmacology and therapeutics : the official journal of the Association for Ocular Pharmacology and Therapeutics.* 2016;32(7):415-424.
20. Tan X, Chen C, Zhu Y, et al. Proteotoxic Stress Desensitizes TGF-beta Signaling Through Receptor Downregulation in Retinal Pigment Epithelial Cells. *Curr Mol Med.* 2017;17(3):189-199.
21. Zhang H, Shang Q, An J, Wang C, Ma J. Crocetin inhibits PDGF-BB-induced proliferation and migration of retinal pigment epithelial cells. *European journal of pharmacology.* 2019;842:329-337.
22. Dvashi Z, Goldberg M, Adir O, Shapira M, Pollack A. TGF-beta1 induced transdifferentiation of rpe cells is mediated by TAK1. *PLoS One.* 2015;10(4):e0122229.
23. Yang J, Li J, Wang Q, Xing Y, Tan Z, Kang Q. Novel NADPH oxidase inhibitor VAS2870 suppresses TGFbetadependent epithelialtomesenchymal transition in retinal pigment epithelial cells. *International journal of molecular medicine.* 2018;42(1):123-130.
24. Dunn KC, Aotaki-Keen AE, Putkey FR, Hjelmeland LM. ARPE-19, a human retinal pigment epithelial cell line with differentiated properties. *Exp Eye Res.* 1996;62(2):155-169.
25. Alge CS, Hauck SM, Priglinger SG, Kampik A, Ueffing M. Differential protein profiling of primary versus immortalized human RPE cells identifies expression patterns associated with cytoskeletal remodeling and cell survival. *Journal of proteome research.* 2006;5(4):862-878.
26. Ahmado A, Carr A-J, Vugler AA, et al. Induction of Differentiation by Pyruvate and DMEM in the Human Retinal Pigment Epithelium Cell Line ARPE-19. *Investigative Ophthalmology & Visual Science.* 2011;52(10):7148-7159.
27. Samuel W, Jaworski C, Postnikova OA, et al. Appropriately differentiated ARPE-19 cells regain phenotype and gene expression profiles similar to those of native RPE cells. *Mol Vis.* 2017;23:60-89.
28. Grierson I, Hiscott P, Hogg P, Robey H, Mazure A, Larkin G. Development, repair and regeneration of the retinal pigment epithelium. *Eye (London, England).* 1994;8 ( Pt 2):255-262.
29. Oganesian A, Bueno E, Yan Q, et al. Scanning and transmission electron microscopic findings during RPE wound healing in vivo. *International ophthalmology.* 1997;21(3):165-175.

# Figures

## Figure 1

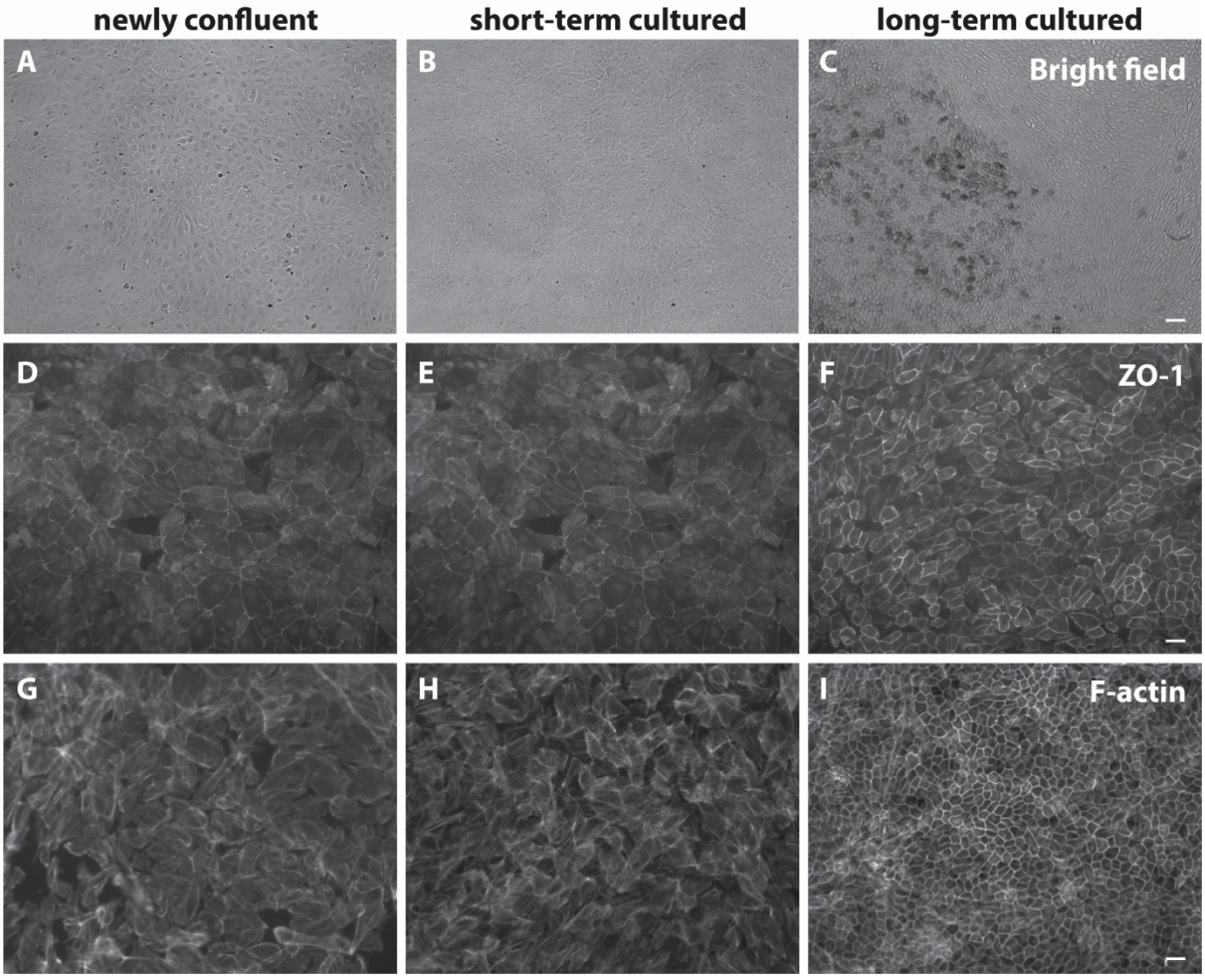

# Figure 2

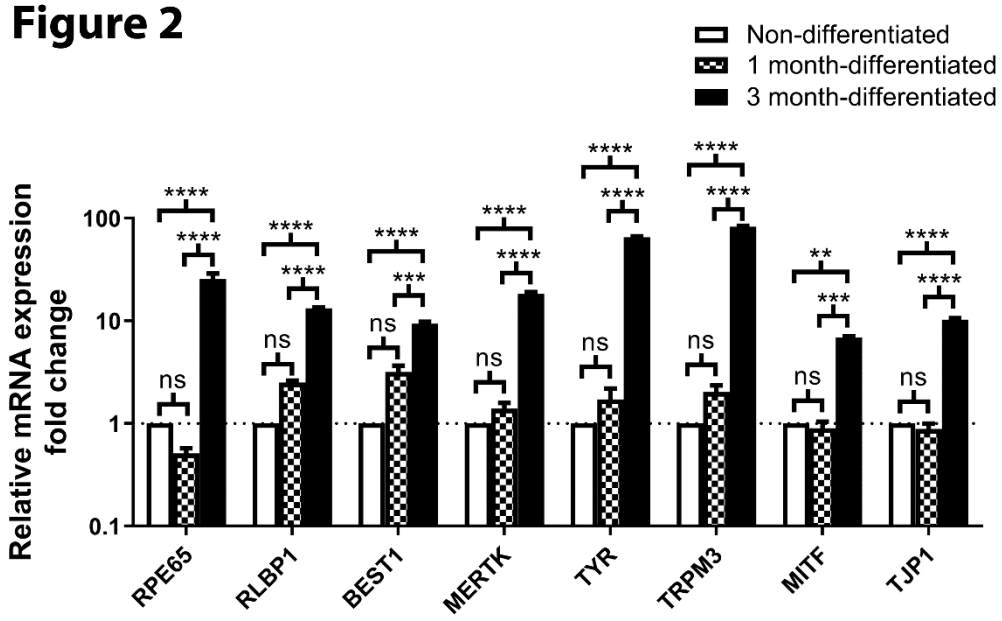
Non-differentiated
1 month-differentiated
3 month-differentiated
Relative mRNA expression
fold change
100
10
1
0.1
****
***
**
ns
RPE65
RLBP1
BEST1
MERTK
TYR
TRPM3
MITF
TJP1

## Figure 3

**A** **Short-term cultured**

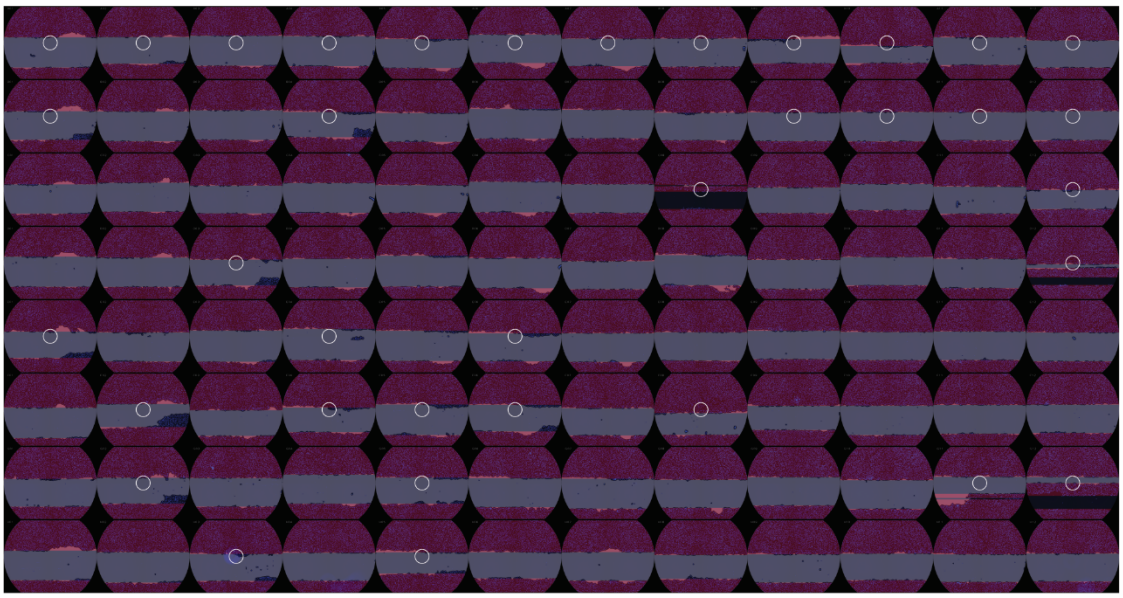

**B** **Long-term cultured**

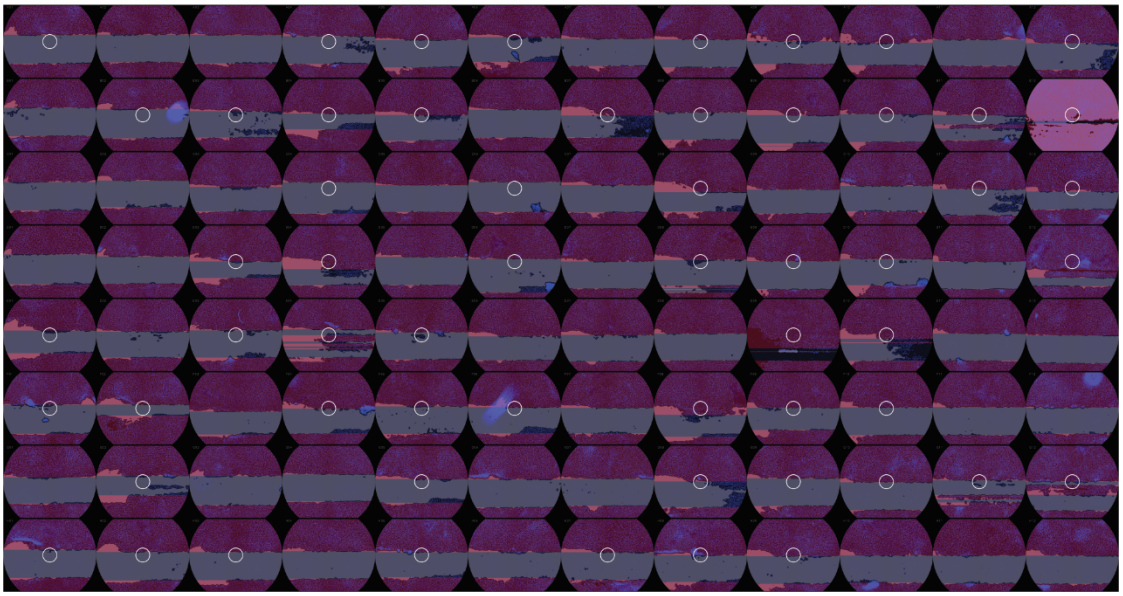

**Figure 4**

**A**

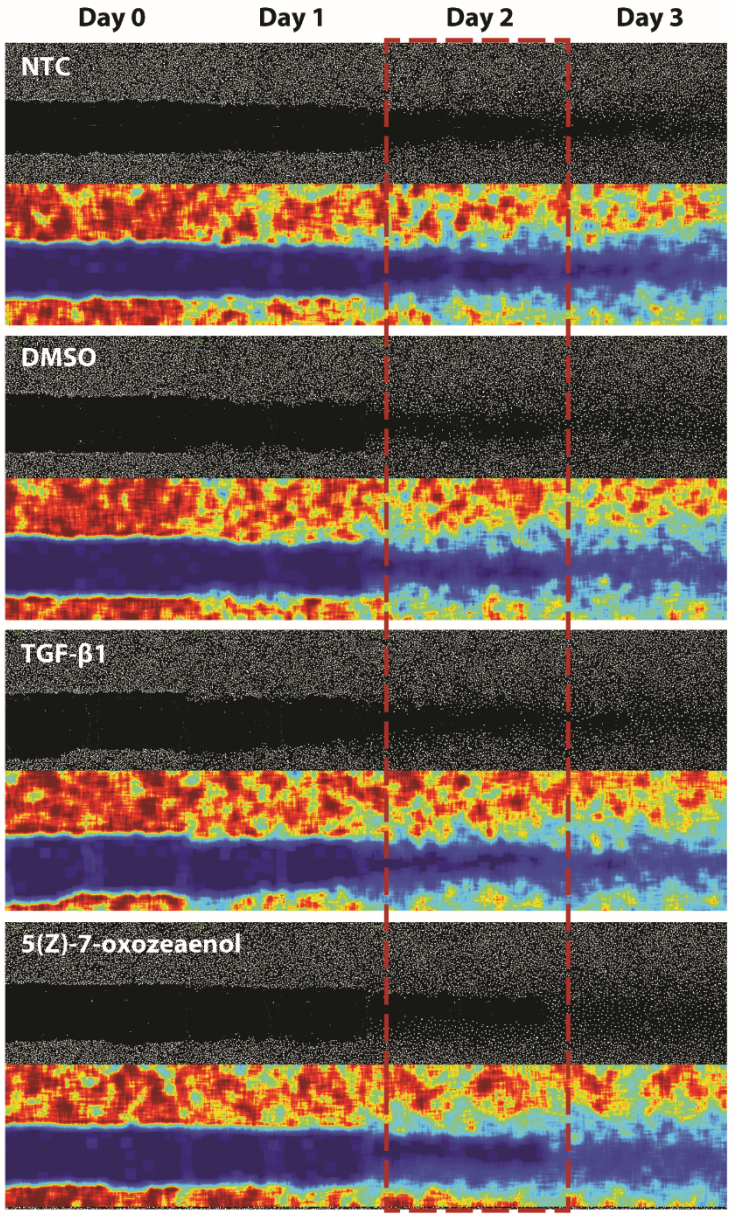
Day 0
Day 1
Day 2
Day 3
NTC
DMSO
TGF-β1
5(Z)-7-oxozeaenol

**B**

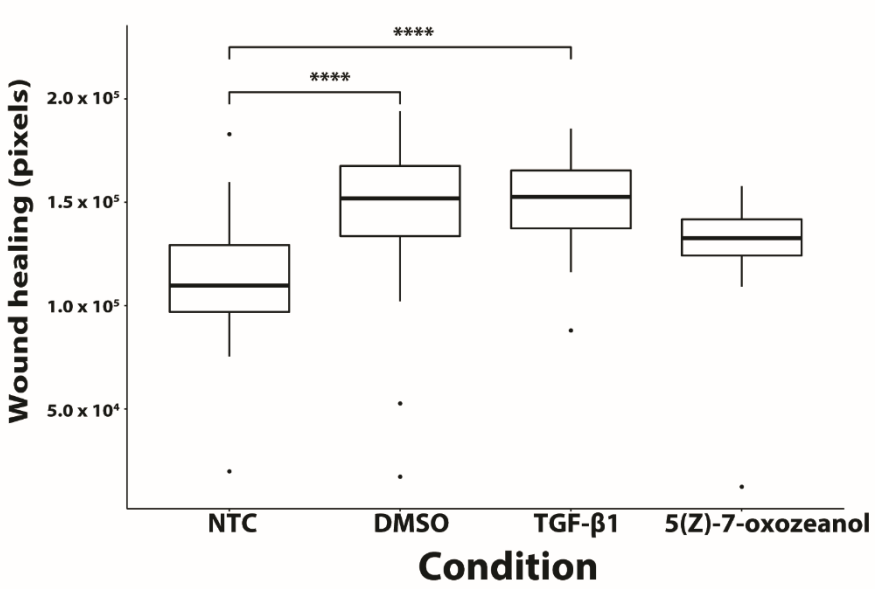
****
****
Wound healing (pixels)
2.0 x 10⁵
1.5 x 10⁵
1.0 x 10⁵
5.0 x 10⁴
NTC
DMSO
TGF-β1
5(Z)-7-oxozeanol
Condition

**Figure 5**

**A**

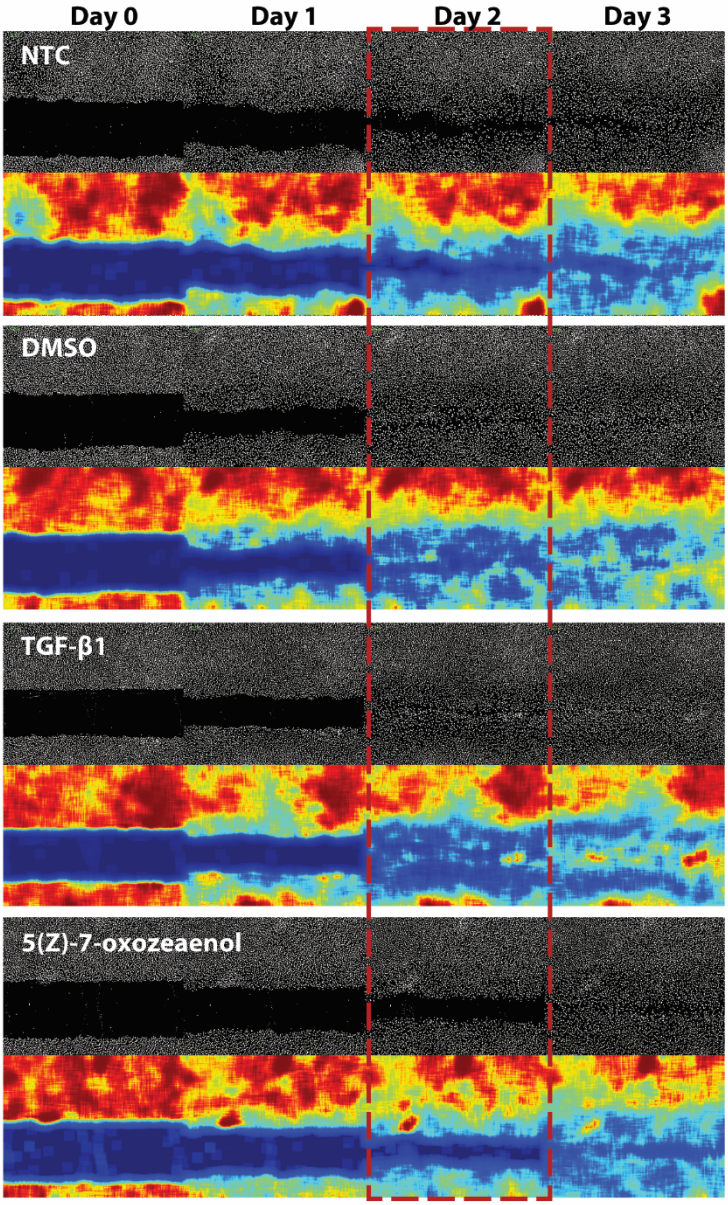
Day 0
Day 1
Day 2
Day 3
NTC
DMSO
TGF-β1
5(Z)-7-oxozeaenol

**B**

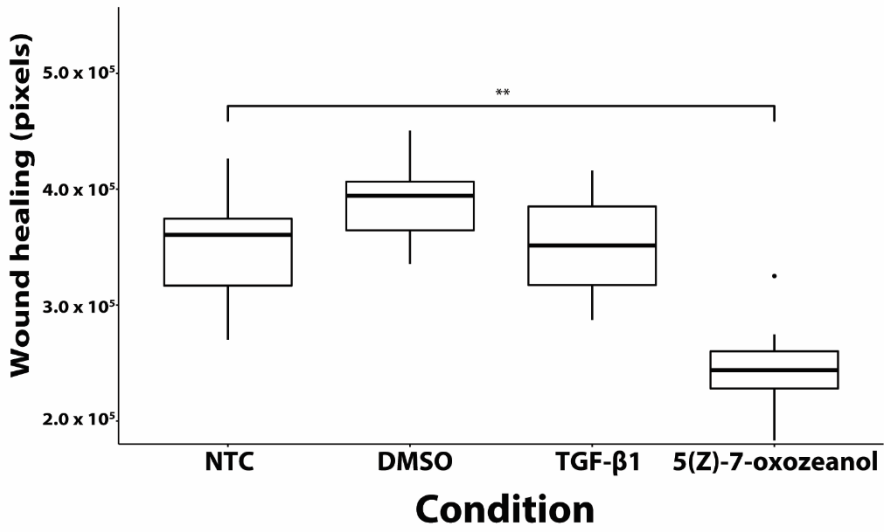
Wound healing (pixels)
5.0 x 10⁵
4.0 x 10⁵
3.0 x 10⁵
2.0 x 10⁵
**
NTC
DMSO
TGF-β1
5(Z)-7-oxozeanol
Condition

# Supplementary Figure 1

**Image processing workflow:**

# Supplementary Figure 2

**A**

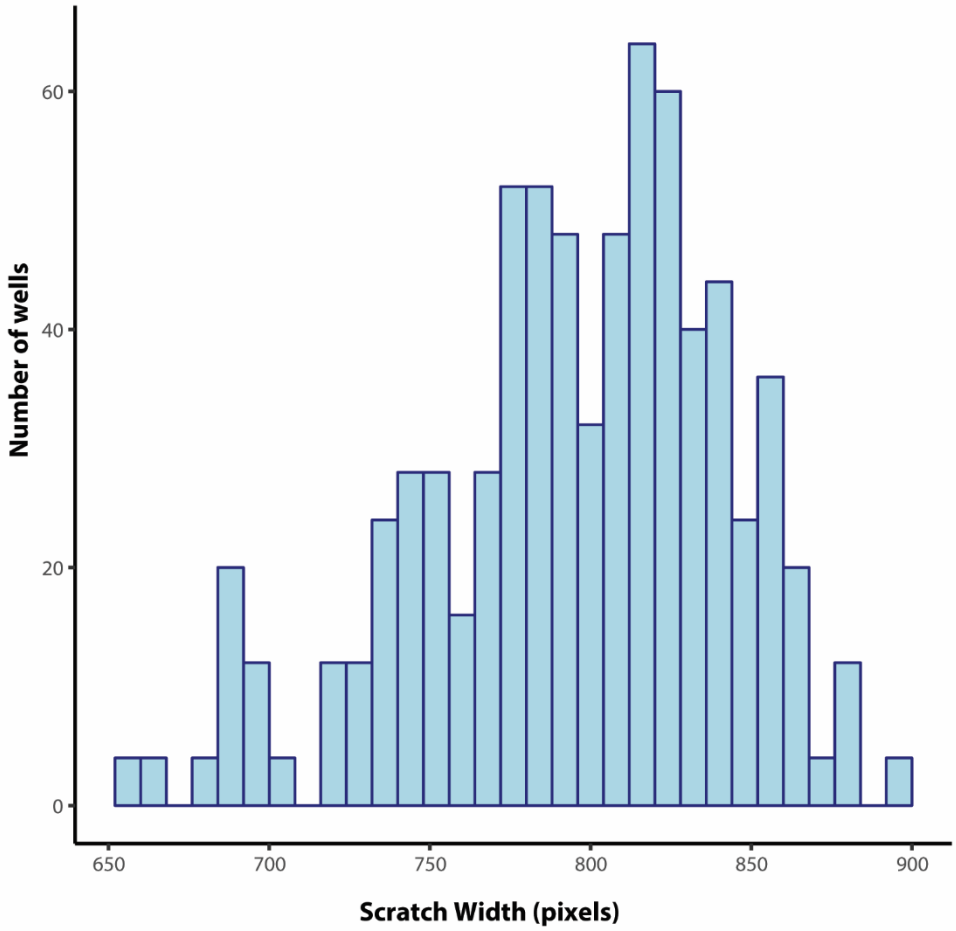


**B**

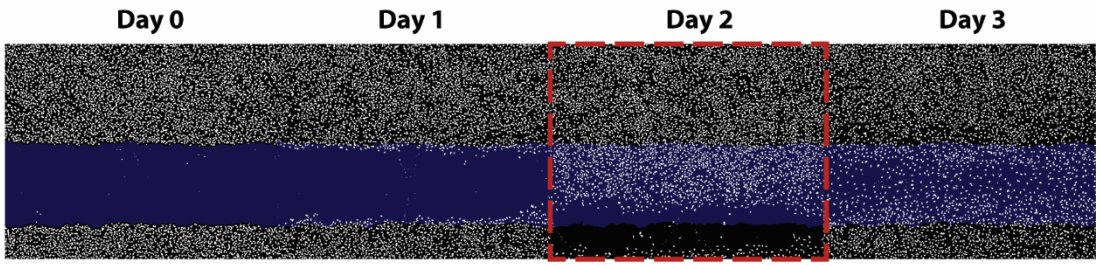

## Supplementary Figure 3

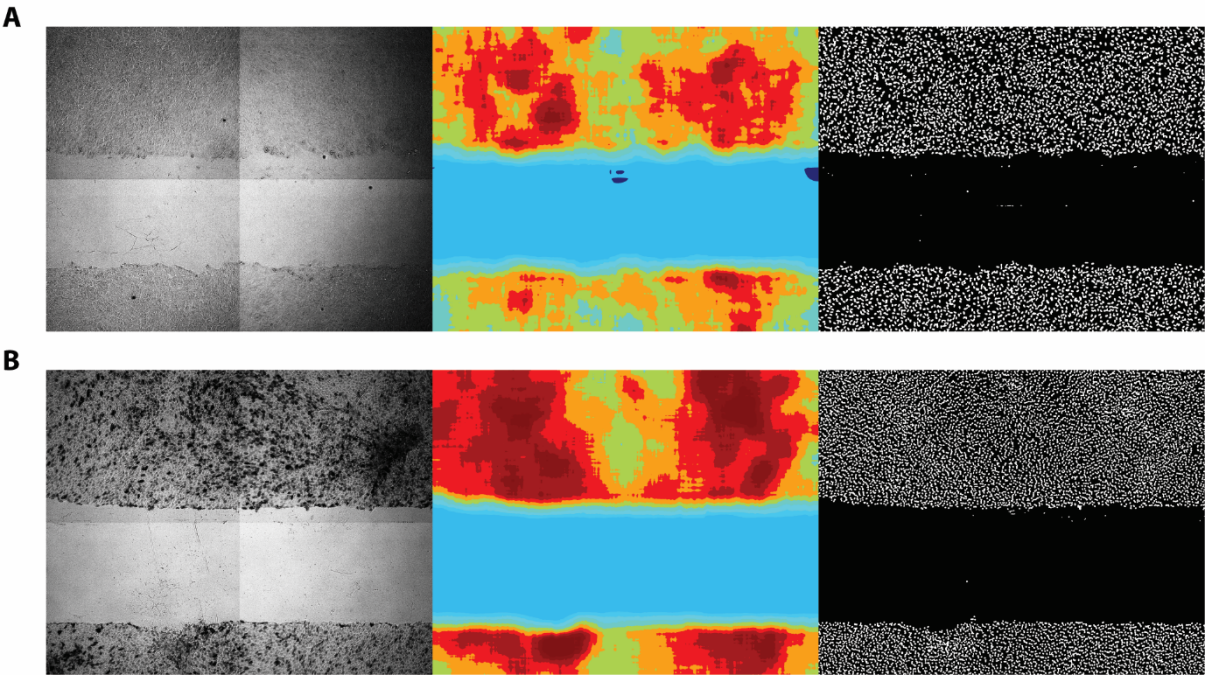

## Text to Figures

**Figure 1** Morphology of newly confluent (A, D and G), short-term (B, E and F) and long-term cultured (C, F and I) ARPE-19 cells visualised using bright field microscopy (A, B and C) (Magnification 10X, scale bar 50 μm) as well as through immunocytochemistry of the tight junction protein ZO-1 (D, E and F) (Magnification 20X, scale bar 25 μm) and filamentous actin (G, H and I) (Magnification 20X, scale bar 25 μm). (I) Filamentous actin stain of highly differentiated patch of ARPE-19 cells. The cells in these patches are densely packed and thus appear smaller than less differentiated cells.

**Figure 2**

Expression of RPE markers in ARPE-19 cells. Total RNA from non-differentiated (white bars), 1 month differentiated (checkered bars) and 3 month differentiated (black bars) ARPE-19 cells was used for qRT-PCR analysis of selected markers for RPE differentiation. Expression levels for selected mRNAs were normalized with GAPDH mRNA levels and shown as fold change relative to the gene expression in non-differentiated ARPE-19 cells. The values are means ± SEM from 3 independent experiments. A Two-way ANOVA found differentiation time was a highly significant factor ($p<0.0001$). The significance of Bonferroni's multiple comparisons test for each gene are shown above each pair of columns. ns = not significant; ** = $p<0.01$; *** = $p<0.01$; **** = $p<0.0001$.

**Figure 3**

Overview of wells containing short-term cultured (A) and long-term cultured (B) ARPE-19 cells at day 0 after wounding. Tiled images from each well have been compiled into a 96-well plate format showing the applied wound segmentation used to exclude wells from wound healing analysis.

Red circles indicate wells that have been excluded from analysis based on wound width <650 pixels and/or scratch smoothness and imaging errors. In total, 86 out of 192 wells were excluded from the

plates with short-term cultured cells; 21 wells based on <658 μm wound width, 66 wells based on scratch smoothness and 15 wells based on imaging errors. 113 out of 192 wells were excluded from the plates with long-term cultured cells; 64 wells based on <650 pixels wound width, 93 wells based on scratch smoothness and 3 wells based on imaging errors. The Kruskal-Wallis test showed no statistical difference of scratch width between plates.

**Figure 4**

*In vitro* wound healing assay of short-term cultured ARPE-19 cells. (A) Overview of the different conditions tested at day 0, 1, 2, and 3. Top panel for each condition shows the thresholded segmented scratch images visualising the distribution of nuclei and the bottom panel heat maps illustrating the nuclei density (blue: low nuclei density and red: high nuclei density) at day 0, 1, 2, and 3. (B) Shows a box plot of the total data set of the relative 'wound healing' for each condition tested at day 2. The horizontal line within the box indicates the median for each data set, the box one standard deviation, and the dots individual outliers. The Kruskal-Wallis rank sum test was applied for statistical analysis. Asterisks indicate statistical significantly different pairs (* = $p<0.05$).

**Figure 5**

*In vitro* wound healing assay of long-term cultured ARPE-19 cells. (A) Overview of the different conditions tested at day 0, 1, 2, and 3. Top panel for each condition shows the thresholded segmented scratch images visualising the distribution of nuclei and the bottom panel heat maps illustrating the nuclei density (blue: low nuclei density and red: high nuclei density) at day 0, 1, 2, and 3. (B) Shows a box plot of the total data set of the relative 'wound healing' for each condition tested at day 2. The horizontal line within the box indicates the median for each data set, the box one standard deviation, and the dots individual outliers. The Kruskal-Wallis rank sum test was applied for statistical analysis. Asterisks indicate statistical significantly different pairs (* = $p<0.05$).

## SUPPLEMENTARY FIGURES

### Supplementary Figure 1

Illustrating the image processing workflow; A) original image (blue: Hoechst nuclear stain visualising the nuclei in the ARPE-19 monolayer , B) output from binary image and mask creation processing workflows of the original image, C) heatmap visualising the cell density (red: high density, blue: low density).

### Supplementary Figure 2

(A) Graph depicting the overall distribution of wound widths measured in all four 96-well plates analysed (1a, 1b, 2a and 2b). (B) Shows an example of an erroneous image acquisition due to failure of the microscope to locate to the exact same region of interest in the well at day 2 resulting in a shift of the wound area and thus incorrect quantification of wound area nuclei. Imaging errors like these resulted in exclusion from the wound healing analysis. The Kruskal-Wallis test showed no statistical difference of scratch width between plates.

### Supplementary Figure 3

(A) Shows a bright field tiled image of the newly wounded area from a well with short-term differentiated ARPE-19 cells at day 0 (left panel) with the corresponding heat map visualisation of nuclei density (middle panel; blue: low nuclei density and red: high nuclei density) and thresholded segmented wound area (right panel). (B) Shows the corresponding images for prolonged differentiated ARPE-19 cells. The heat map and the thresholded segmented wound area images clearly illustrate a higher nuclei density in the prolonged differentiated wells.

**Text to Tables**

**Table 1.**

TaqMan Probes used for qRT-PCR expression analysis of RPE markers.